Mechanical Performance of Short Models for MQXF, the Nb3Sn Low-β Quadrupole for the Hi-Lumi LHC

G. Vallone, G. Ambrosio, E. Anderssen, N. Bourcey, D. W. Cheng, H. Felice, P. Ferracin, C. Fichera, P. Grosclaude, M. Guinchard, M. Juchno, H. Pan, J.C. Perez, S. Prestemon

***Abstract*— In the framework of the Hi-Lumi LHC project, CERN and US LARP are jointly developing MQXF, a 150 mm aperture high-field Nb3Sn quadrupole for the upgrade of the inner triplet of the low-beta interaction regions. The magnet is supported by a shell-based structure, providing the preload by means of bladder-key technology and differential thermal contraction of the various components. Two short models have been produced using the same cross-section currently considered for the final magnet. The structures were preliminarily tested replacing the superconducting coils with blocks of aluminum. This procedure allows for model validation and calibration, and also to set performance goals for the real magnet. Strain gauges were used to monitor the behavior of the structure during assembly, cool-down and also excitation in the case of the magnets. The various structures differ for the shell partitioning strategies adopted and for the presence of thick or thin laminations. This paper presents the results obtained and discusses the mechanical performance of all the short models produced up to now.**

***Index Terms*—Hi-Lumi LHC, LARP, Nb3Sn magnet, quadrupole, short model.**

I. Introduction

The High Lumi LHC project has the scope of enabling the integrated luminosity threshold of 3000 fb^{-1}[1]. A crucial part of the upgrade is the enhancement of the triplet regions, where the MQXF magnet will be used in Q1, Q2 and Q3 quadrupoles. These quadrupoles are developed in a collaboration between CERN and the US-LARP (LHC Accelerator Research Program). The magnet will be produced in two lengths, MQXFA and MQXFB, with a magnetic length of 4.2 m and 7.15 m respectively [2]. Currently, a series of short models, with a magnetic length of 1.2 m, is being tested both at CERN and LARP. This paper analyzes the mechanical performance of the structure: after a summary of the magnet features, the mechanical performance validation is described. First, coil stress measurements were validated with respect to analysis. Measures from two different systems were compared. Then, the support structures were tested, demonstrating that the structure can provide a precise and uniform prestress to the coils. Finally, the mechanical behavior of the first short magnet was studied, with respect to prestress and performance during excitation.

Automatically generated dates of receipt and acceptance will be placed here;
This work was supported by the High Luminosity LHC Project at CERN and by the DOE through the U.S. LHC Accelerator Research Program.

G. Vallone, N. Bourcey, P. Ferracin, C. Fichera, P. Grosclaude, M. Guinchard and J.C. Perez are with the European Organization for Nuclear Research (CERN), 1211 Geneva, Switzerland (e-mail: giorgio.vallone@cern.ch).

G. Ambrosio is with the Fermi National Accelerator Laboratory, Batavia, IL 80510 USA.

H. Felice is with the French Atomic Energy Commission, 91400 Saclay, France.

E. Anderssen, D. W. Cheng, M. Juchno and S. Prestemon are with Lawrence Berkeley National Laboratory, Berkeley, CA 94720 USA.

Colour versions of one or more of the figures in this paper are available online at http://ieeexplore.ieee.org.
Digital Object Identifier: xx

II. Magnet Features Description

The MQXF magnet cross-section, used for both short and long prototypes, is shown in Fig. 1. The desired prestress is reached in two steps. First, the bladder-key technology [3] is used to preload the coil at room-temperature. Then, during the cool-down to cryogenic temperatures, the differential thermal contraction coefficients of the structure components further

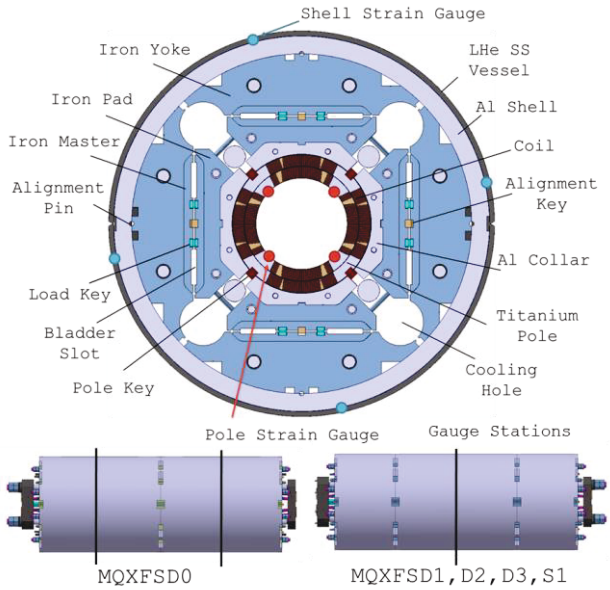

Fig. 1. Cross section of MQXF magnets. Strain Gauges locations on shell and poles are shown. Cross-sectional coil gauge position is the same for the mechanical models with dummy coils. Vertical lines denote the axial position of the strain gauges.

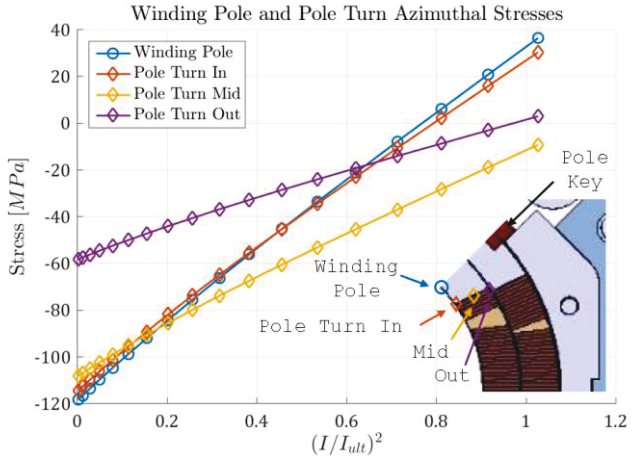

Fig. 2. Computed stresses during excitation on the inner radius of the winding pole, where strain gauges are installed, and on three locations of the pole turn. The computation shows that the measured stress is very representative of the pole turn stress on the inner radius.

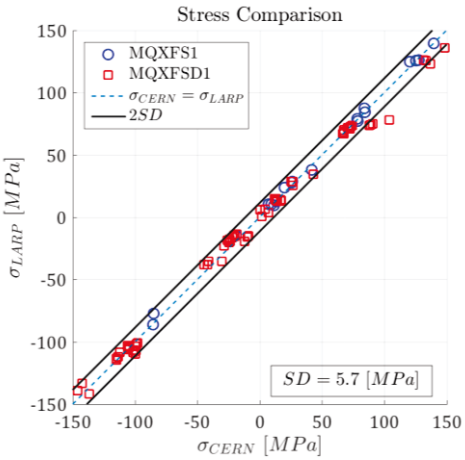

Fig. 3. MQXFS1 and MQXFSD1 stresses, as computed from LARP and CERN systems measured strains. Each data point corresponds to a particular location and a particular instant. For a ±150 MPa measure range, the stresses were confined in a band of ±10 MPa.

increase the prestress to the desired value. The prestress is controlled by the amount of shimming inserted on eight loading keys, while the thermal contraction contribution is considered constant. A detailed description of the magnet cross section design can be found in [4].

The first 1.5 m long mechanical structure, made by 50 mm thick laminations and produced at CERN, was initially tested with two 0.7 m long shells and aluminium coils (MQXFSD0 [5], see also Fig. 1). It can be shown that the coil azimuthal stress has a minimum at the position of a cut between two shell sections. With the original partitioning strategy, this minimum was undesirably at the axial coil center. As a consequence, the structure was then reassembled with two lateral shells, 0.4 m long, and one 0.7 m long central shell (MQXFSD2). Further details about the influence of shell partitioning over coil stress can be found in [6]. An equivalent three-shell structure, produced at LARP, was tested with dummy coils (MQXFSD1) and then with real coils, in the first short model MQXFS1. Magnet parameters are reported in [7]. Finally, a thin laminated structure was produced at CERN and tested with dummy coils (MQXFSD3). In this structure iron yoke and pads are made of stacks of 5.8 mm laminations. The structure is currently being used to assembly the MQXFS3 magnet. Because of the associated cost reduction, thin laminations are considered the baseline for the final magnets.

III. Strain Gauge Measurements

A. Instrumentation Description

Strain gauges were installed on all the models, on the positions shown in Fig. 1 and Fig. 2. Longitudinal gauges were also installed on the aluminium rods.

The shell and pole gauges are used to monitor the azimuthal force provided by the structure and its result in terms of coil pre-stress. Since measurements from strain gauges installed directly on the coil are considered less reliable [8], the coil stress is indirectly monitored measuring the winding pole stress. To verify if this measure is representative of the coil stress, the computed winding pole stress was compared to the pole turn stresses in three locations. Results, reported in Fig. 2, show that the winding pole stress is very close to the pole turn stress at the inner radius. This value is particularly interesting, being the coil peak stress after cooldown and the first one to undergo tension during excitation.

B. Measurement Comparison

On MQXFSD1 and MQXFS1, two strain measuring systems were used, one provided by LARP and one by CERN. In both cases, gauges were bridged with a compensator, attached to a separate piece of titanium for the poles or aluminum for shell and dummy coils. The LARP system was powered in DC and used Vishay gauges in full bridge configuration. The CERN system used HBM modules and gauges, connected in half bridge configuration. Both AC and DC voltage powering strategies were tested. While it is not within the scope of the present paper to study the differences between the two systems in detail, the comparison between the readings can provide an indication of the absolute precision of the systems.

Fig. 3 shows the stress computed in the same location, at the same instant, using the azimuthal and longitudinal strains provided by the CERN and LARP systems after loading and cooldown. There is no evident systematic deviation of the measurements. In a range of ±150 MPa, measurement difference is always in a band of ±10 MPa, equal to two times the Standard Deviation SD. This result provides a reference for the comparison of stresses on different quadrants, as well as computed and measured values.

IV. Prestress Analysis

Key aspects of the mechanical structure performance are the control on the average pre-stress and its variation on the different quadrants.

A. Average Azimuthal Prestress

The shell is providing the total azimuthal prestress: part of it compresses the pole, and then flows to the coil with the relationships shown in Fig. 2; the rest compresses the pole key. This feature is used to guarantee the alignment of the coil to the structure [2]. In line of principle, the pole key will not always

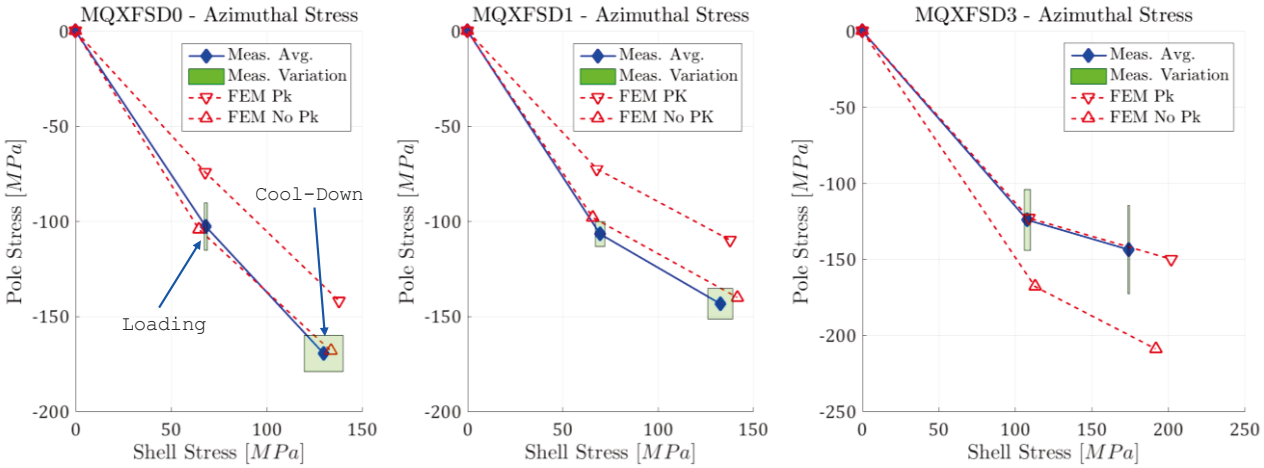

Fig. 4. Transfer Function plot for the mechanical models with dummy coils. Three lines are plotted: the measured average and the FE results with or without the pole key in contact on the collar sides. The lines depict three different points: before loading (zero), after loading, and after cooldown. The green area represents the measured stress variation. Left: MQXFSD0. Centre: MQXFSD1. The pole key is considered not in contact. Right: MQXFSD3. The pole key is considered in contact.

be locked in place by the side of the collars. This would be the case when, for example, the collars gap is bigger than expected. Also, a twisted coil could force the pole key to be in contact only on one collar side, carrying no azimuthal force.

A useful tool to study the accuracy of numerical model estimates is the Transfer Function (TF) between the shell and pole stresses. The result for such TF is shown in Fig. 4 for MQXFSD0, MQXFSD1 and MQXFSD3, after key insertion and at the end of the cool-down. The plot for MQXFSD2 is not shown since the structure is completely equivalent to MQXFSD1. Two different FE models are compared against the experimental data: one, assuming the pole key is in direct contact with the collars, and one, neglecting this contact. For both models the azimuthal shell strain after loading is matched varying the loading key interference. It is clear that for a given shell tension, the pole compression will be higher when the pole key is not in contact with the collars. As a consequence, the TF can be used not only as a model validation tool, but also to evaluate the actual alignment of the coils. The distance between the two model TF measures the amount of prestress needed to guarantee the alignment.

In MQXFSD0, MQXFSD1 and MQXFSD2, the measured values were always closer to the predictions of the model without the pole key. Because of this, during the MQXFSD3 assembly, the pole-key azimuthal shimming was increased by 100 µm. As shown in Fig. 4, the TF moved as desired towards the pole key model. This assembly also validated the thin laminated structure. To produce the results shown in Fig. 4, an increase in the friction coefficients was needed. This may be due to the rough contact generated by the thin laminations.

In MQXFSD1, MQXFSD2 and MQXFSD3 a small inconsistency with the models was observed: the measured shell stress increase during cooldown is always lower than the computed one. This effect is not explained at the moment, but can be easily compensated by increasing the amount of shimming on the loading keys, hence the pre-load at room temperature.

When the aluminium blocks were substituted with the real coils in MQXFS1, similar agreement was expected. Surprisingly, the comparison with the model was not satisfactory: as shown in Fig. 5, the TF did not match the model slope both during loading and cool-down. The mechanical

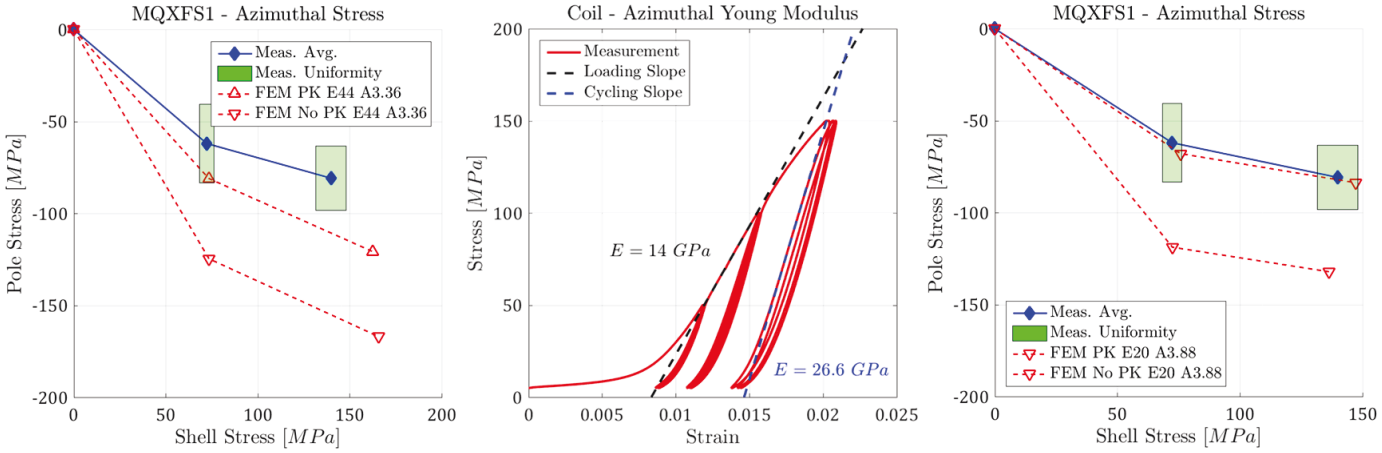

Fig. 5. Left: MQXFS1 TF plot, using a 44 GPa coil elastic modulus. While the model does not match the experimental data, it can already be concluded that the pole key is in contact. Centre: Preliminary measurement of the MQXFS coil elasticity modulus in the azimuthal direction. Compression test was performed at room temperature and in free-free conditions. The material shows two different slopes when increasing the maximum stress reached on the virgin specimen, and during subsequent loading cycles. Right: MQXFS1 TF plot, using the new coil properties. Both shell and coil computed stresses are now within the measured variation.

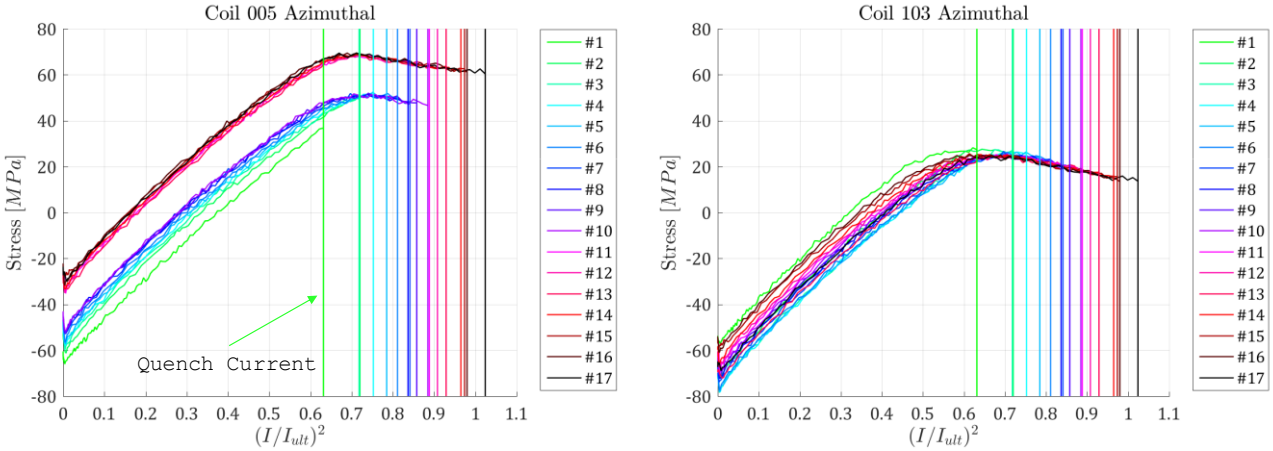

Fig. 6. Left: Coil 005 pole azimuthal stress during training. The vertical lines mark the quench current of each ramp. The strain exhibits an almost constant linear zone, followed by a progressively extending flat one. Right: Coil 103 pole azimuthal stress during training, computed using the longitudinal strain from Coil 005 pole.

model experience suggested that the model inaccuracy could be traced back to the used coil mechanical properties. It can be shown that the transfer function does not depend strongly on the coil elastic modulus only when the g10 pole key is not in contact with the collars. This is a consequence of the direct force exchange between shell and the coil poles. On the other hand, when the pole key and collar are in direct contact, the pole key shares the available shell azimuthal force as a spring in parallel with the coil, thus varying the slope as a function of their stiffness ratio.

A parametric analysis was then performed, varying the elastic modulus of the coil. The analysis showed that it is possible to match the measured loading TF moving from a modulus of 44 GPa, as used in [7], to 20 GPa. Also, to match the stress after cool-down a variation of the thermal integrated contraction was required: from 3.16 mm to 3.88 mm. In the meantime, an experimental campaign was launched to measure the elastic modulus on ten stacks specimens. Preliminary measurements of Fig. 5 show a different modulus for the loading and cycling phases: respectively 14 and 26 GPa. This averages at 20 GPa, that is very close to the value obtained from the simulations. However, this result was obtained on a single specimen and has still to be confirmed by the measurement campaign. The TF computed using the new modulus, shown in Fig. 5, is now close to the measured one.

B. *Prestress Variation*

For all the experiments, stress variations were measured across the four quadrants. These differences could be introduced, for example, by tolerances in components and assembly. After cooldown, the shell stress variation was within ±10 MPa for MQXFSD0, ±7 MPa for MQXFSD1, and negligible for MQXFSD3. Consistent variations were measured on the four aluminium dummy coil blocks: ±10 MPa for MQXFSD0, ±8 MPa for MQXFSD1. As evident in Fig. 4, the variation was much higher in the case of MQXFSD3 dummy coils. The four measured stresses were 153, 156, 162 and 104 MPa. The variation is equal to ±30 MPa, but is clear that this effect is limited to a single block. It is worth to notice that the MQXFSD0 and MQXFSD1 stress variation on both shell and poles is smaller than the difference of the measurements of LARP and CERN systems.

MQXFS1 shell performed similarly: the values were within ±9 MPa. On the other hand, the coil azimuthal stresses were within a ±17 MPa band. This greater variation was expected, since the coil geometrical precision is much lower than the one of the dummy blocks [9]. In general, results using mechanical models with dummy coils should be considered as a reference value for achievable stress uniformity.

V. MQXFS1: Magnet Excitation

The MQXFS1 magnet underwent 17 training quenches to reach ultimate current. Quench current gradually increased from 14.1 kA to the ultimate value, equal to 17.8 kA [10]. The training was then stopped to allow for a reloading operation, whose results will be presented in the future. The magnet also underwent a thermal cycle after training: ultimate current was reached without further quenches, showing full memory. Further information can be found in [10].

A. *Pole Azimuthal Stress during Excitation*

Pole stresses during subsequent ramps are shown in Fig. 6, where vertical lines are used to track the quench currents. The signals exhibit a marked division in two zones: in the first zone,

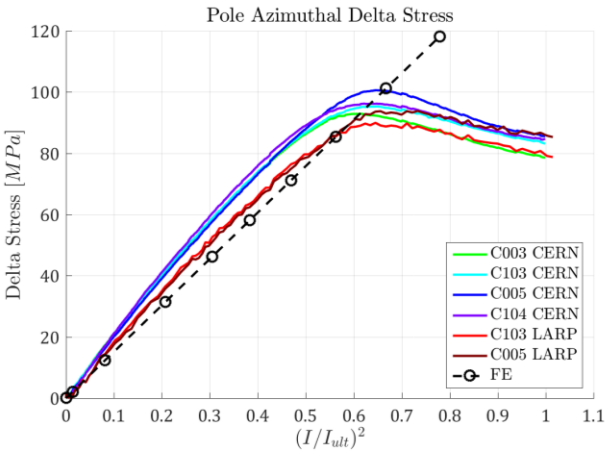

Fig. 7. Measured pole azimuthal stress during the last ramp. Remarkable uniformity is found on the overall prestress shown by the four coils. Also, no significant difference is found between the results from the two systems. The FE model results are in agreement with the linear part.

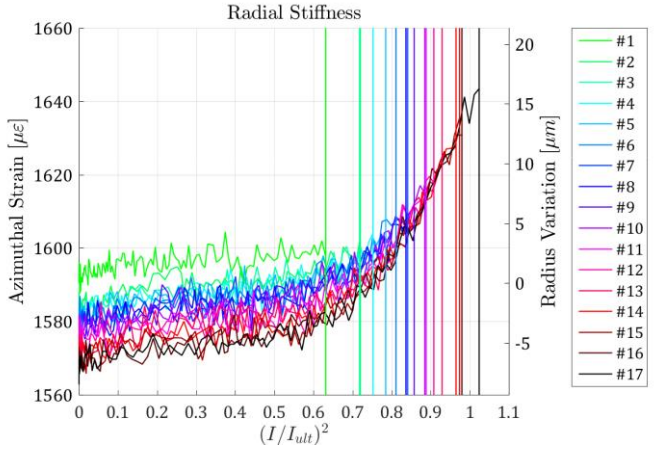

Fig. 8. Shell radius variation during excitation, computed from the azimuthal strain. The signals show the same division in two zones observed on the poles. During the last ramp, the radius increase was equal to 23 μm.

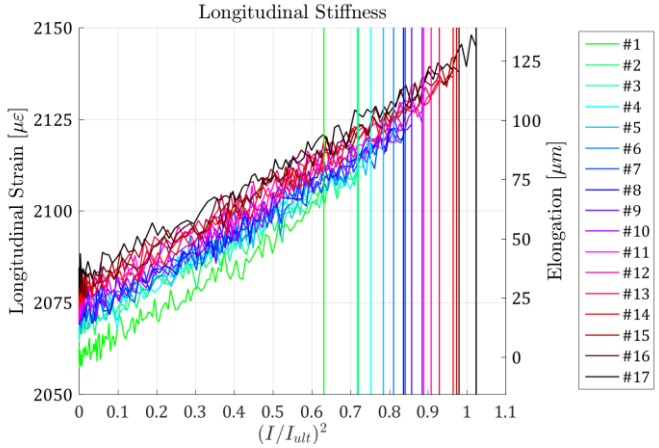

Fig. 9. Rods elongation during excitation. Their free length, initially equal to 1550 mm, increased by 96 μm during excitation. Because of the magnet configuration, this value is equal to the coil longitudinal elongation.

the pole is gradually unloaded; then, the signal bends and gradually decreases. This is generally considered an indication of detachment of the coil from the pole, and in general of low prestress [11], [12]. The negative slope after the plateau was unexpected and is under investigation.

Ratcheting was also observed, with a progressive reduction of the azimuthal stress after each ramp. In addition, after certain ramps the stresses were subject to jumps in both directions. After these jumps, Coil 005 reached a plateau tension higher than 60 MPa. This would not be compatible with the coil/pole bonding, as the epoxy breaking tension is commonly assumed between 0 and 20 MPa [12], and may be an indication of a non-physical offset in the gauge measures.

The azimuthal stress during the last ramp is shown in Fig. 7. As not all the longitudinal strains were available, some of the stresses were computed considering the average value of longitudinal strains on the other coils. The associated effect is considered to be small, both because of the entity of longitudinal strain variations and their minor effect on the azimuthal stress. The difference between LARP and CERN systems values during excitation is very small: at ultimate current the difference is lower than 5 MPa on coil 103 and negligible on coil 005. From the maximum delta stress, it is possible to roughly estimate the average effective prestress between 90 and 100 MPa. This is close to the measured value after cooldown, 81 MPa (see Fig. 5, right). The variation across different coils was very small if compared to the one after cooldown: maximum delta stresses in Fig. 7 are within a ±5 MPa band. This result suggests that, during the training, the prestress is redistributed more uniformly.

FE model was able to reproduce only the slope of the linear part: this is consistent with the hypothesis that the coil is detaching from the pole, as the model considers them glued.

B. Shell and Rods: Structure Stiffness

An important factor in the evaluation of the mechanical performance is the overall structure stiffness: how much it can deform under the applied loads. Assuming that the shell always remains circular, the azimuthal strain can be used to compute its radius variation. Results during excitation are reported in Fig. 8. The radius was initially equal to 307 mm. The increase during excitation was limited to 23 μm. Similarly, the longitudinal strain in the rods allows for the computation of their elongation, shown in Fig. 9. Since the rods and coils are directly connected, the rod elongation is equal to that of the coil pack. The free length of the rods was equal to 1550 mm. During excitation, the maximum elongation was equal to 96 μm. Finally, a ratcheting effect produced 35 μm of permanent elongation during the training quenches.

VI. Conclusion

In this paper, the authors presented the mechanical performance of MQXFS structures tested so far. Support structures demonstrated that they are capable of applying the required prestress to the coil. The MQXFSD3 experiment also validated the usage of the thin laminations, providing 143 MPa of azimuthal prestress to the aluminium blocks. For all the experiments, variations of azimuthal stresses on the shells were always lower than ±10 MPa. The same result was achieved for the aluminium blocks when substituted for the the coils in the mechanical models. In MQXFS1, the real coil stress variation was equal to ±17 MPa. After the training, the stresses redistributed across the quadrants, and the different poles showed a variation of ±5 MPa. Clear unloading of the poles was seen during excitation. This allowed to estimate an effective prestress between 90 and 100 MPa, which was close to the measured value after cooldown, 81 MPa. The unloading did not compromise the structure rigidity, as the maximum radial displacement during excitation was 23 μm, and the maximum elongation of the coil was 35 μm. Finite Element models were proven to be an accurate tool not only to control the applied prestress but also to evaluate the alignment of the coil to the structure. For the MQXFS1 magnet this required a variation of the coil elastic modulus, confirmed by preliminary measurements.

References

[1] L. Rossi and O. Brüning, "High Luminosity Large Hadron Collider A description for the European Strategy Preparatory Group," CERN-ATS-2012-236, 2012.

[2] P. Ferracin, G. Ambrosio, M. Anerella, A. Ballarino, H. Bajas, M. Bajko, B. Bordini, R. Bossert, D. W. Cheng, D. R. Dietderich, G. Chlachidze, L.

Cooley, H. Felice, A. Ghosh, R. Hafalia, E. Holik, S. Izquierdo Bermudez, P. Fessia, P. Grosclaude, M. Guinchard, M. Juchno, S. Krave, F. Lackner, M. Marchevsky, V. Marinozzi, F. Nobrega, L. Oberli, H. Pan, J. C. Perez, H. Prin, J. Rysti, E. Rochepault, G. Sabbi, T. Salmi, J. Schmalzle, M. Sorbi, S. Sequeira Tavares, E. Todesco, P. Wanderer, X. Wang, and M. Yu, "Development of MQXF: The Nb3Sn Low-β Quadrupole for the HiLumi LHC," IEEE Trans. Appl. Supercond., vol. 26, no. 4, pp. 1–7, 2016.

[3] S. Caspi, S. Gourlay, R. Hafalia, A. Lietzke, J. Oneill, C. Taylor, and A. Jackson, "The use of pressurized bladders for stress control of superconducting magnets," IEEE Trans. Appl. Supercond., vol. 11, no. 1 II, pp. 2272–2275, 2001.

[4] P. Ferracin, G. Ambrosio, M. Anerella, F. Borgnolutti, R. Bossert, D. Cheng, D. R. Dietderich, H. Felice, A. Ghosh, A. Godeke, S. I. Bermudez, P. Fessia, S. Krave, M. Juchno, J. C. Perez, L. Oberli, G. Sabbi, E. Todesco, and M. Yu, "Magnet Design of the 150 mm Aperture Low-β Quadrupoles for the High Luminosity LHC," IEEE Trans. Appl. Supercond., vol. 24, no. 3, pp. 1–6, 2014.

[5] M. Juchno, G. Ambrosio, M. Anerella, H. Bajas, M. Bajko, N. Bourcey, D. W. Cheng, H. Felice, P. Ferracin, P. Grosclaude, M. Guinchard, J. C. Perez, H. Prin, and J. Schmalzle, "Mechanical Qualification of the Support Structure for MQXF, the Nb3Sn Low-β quadrupole for the high luminosity LHC," IEEE Trans. Appl. Supercond., vol. 26, no. 4, 2016.

[6] M. Juchno, G. Ambrosio, M. Anerella, D. Cheng, H. Felice, P. Ferracin, J. C. Perez, H. Prin, and J. Schmalzle, "Support Structure Design of the Nb3Sn Quadrupole for the High Luminosity LHC," IEEE Trans. Appl. Supercond., vol. 25, no. 3, pp. 1–4, 2015.

[7] H. Pan, H. Felice, D. W. Cheng, E. Anderssen, G. Ambrosio, J. C. Perez, M. Juchno, P. Ferracin, and S. O. Prestemon, "Assembly Tests of the First Nb3Sn Low-β Quadrupole Short Model for the Hi-Lumi LHC," IEEE Trans. Appl. Supercond., vol. 26, no. 4, pp. 1–5, Jun. 2016.

[8] S. Caspi, S. E. Bartlett, D. R. Dietderich, P. Ferracin, S. A. Gourlay, C. R. Hannaford, A. R. Hafalia, A. F. Lietzke, S. Mattafirri, M. Nyman, and G. Sabbi, "Measured strain in Nb3Sn coils during excitation and quench," IEEE Trans. Appl. Supercond., vol. 15, no. 2 PART II, pp. 1461–1464, 2005.

[9] E. F. Holik, G. Ambrosio, M. Anerella, R. Bossert, E. Cavanna, D. Cheng, D. R. Dietderich, P. Ferracin, A. K. Ghosh, S. Izquierdo Bermudez, S. Krave, A. Nobrega, J. C. Perez, I. Pong, E. Rochepault, G. L. Sabbi, J. Schmalzle, and M. Yu, "Fabrication and Analysis of 150-mm-Aperture Nb3Sn MQXF Coils," IEEE Trans. Appl. Supercond., vol. 26, no. 4, 2016.

[10] G. Chlachidze, G. Ambrosio, M. Anerella, R. Bossert, E. Cavanna, D. Cheng, D. Dietderich, J. DiMarco, H. Felice, P. Ferracin, A. Ghosh, P. Grosclaude, M. Guinchard, A. R. Hafalia, E. Holik, S. Izquierdo Bermudez, S. Krave, M. Marchevsky, F. Nobrega, D. Orris, H. Pan, J. C. Perez, S. Prestemon, E. Ravaioli, G. Sabbi, T. Salmi, J. Schmalzle, S. Stoynev, T. Strauss, C. Sylvester, M. Tartaglia, E. Todesco, G. Vallone, G. Velev, P. Wanderer, X. Wang, M. Yu, "Performance of the first short model 150 mm aperture Nb3Sn quadrupole MQXFS for the High-Luminosity LHC," in IEEE Trans. Appl. Supercond., this conference.

[11] P. Ferracin, G. Ambrosio, M. Anerella, B. Bingham, R. Bossert, S. Caspi, D. W. Cheng, G. Chlachidze, H. Felice, A. R. Hafalia, W. Mumper, F. Nobrega, S. Prestemon, G. L. Sabbi, J. Schmalzle, C. Sylvester, M. Tartaglia, P. Wanderer, and A. V. Zlobin, "Mechanical Performance of the LARP Nb3Sn Quadrupole Magnet LQS01," IEEE Trans. Appl. Supercond., vol. 21, no. 3, pp. 1683–1687, Jun. 2011.

[12] H. Felice, G. Ambrosio, M. Bajko, E. Barzi, B. Bordini, R. Bossert, S. Caspi, D. Dietderich, P. Ferracin, J. Feuvrier, A. Ghosh, A. Godeke, J. Lizarazo, L. Rossi, G. Sabbi, P. Wanderer, X. Wang, and A. V Zlobin, "Test results of TQS03: A LARP shell-based Nb 3 Sn quadrupole using 108/127 conductor," J. Phys. Conf. Ser., vol. 234, no. 3, p. 32010, Jun. 2010.